PROCEEDINGS OF SCIENCE

The lower moments of nucleon structure functions in lattice QCD with physical quark masses

Ryutaro Tsuji,[†,a,*] **Yasumichi Aoki,**[b] **Ken-Ichi Ishikawa,**[c] **Yoshinobu Kuramashi,**[d] **Shoichi Sasaki,**[a] **Eigo Shintani**[d] **and Takeshi Yamazaki**[e,d]

(PACS Collaboration)

[a] *Department of Physics, Tohoku University, 980-8578,Sendai, Japan*

[b] *RIKEN Center for Computational Science, 650-0047, Kobe, Japan*

[c] *Core of Research for the Energetic Universe, Graduate School of Advanced Science and Engineering, 739-8526, Higashi-Hiroshima, Japan*

[d] *Center for Computational Sciences, University of Tsukuba, 305-8577, Tsukuba, Japan*

[e] *Faculty of pure and Applied Sciences, University of Tsukuba, 305-8571, Tsukuba, Japan*

E-mail: tsuji@nucl.phys.tohoku.ac.jp

We present results for the nucleon structure functions and form factors obtained from 2+1 flavor lattice QCD with physical light quark masses (m_π = 135 MeV) in a large spatial extent of about 10 fm. Our calculations are performed with the PACS10 gauge configurations generated by the PACS Collaboration with the six stout-smeared $\mathcal{O}(a)$ improved Wilson-clover quark action and Iwasaki gauge action at β = 1.82 and 2.00 corresponding to lattice spacings of 0.085 fm and 0.064 fm respectively. The lower moments of structure functions, $\langle x \rangle_{u-d}$ and $\langle x \rangle_{\Delta u - \Delta d}$ given by the twist-2 operators being properly renormalized, are evaluated in the $\overline{\text{MS}}$ scheme at the renormalization scale of 2 GeV only at β = 1.82, since the renormalization factors at β = 2.00 have not yet determined nonperturbatively in the RI/MOM scheme. Instead, at two lattice spacings, we evaluate appropriate ratios of g_A/g_V and $\langle x \rangle_{u-d}/\langle x \rangle_{\Delta u - \Delta d}$, which are not renormalized in the continuum limit. These quantities thus can be directly compared with the experimental data without the renormalization.

The 38th International Symposium on Lattice Field Theory, LATTICE2021 26th-30th July, 2021 Zoom/Gather@Massachusetts Institute of Technology

[†] Present adress is *RIKEN Center for Computational Science, 650-0047, Kobe, Japan.*

[*] Speaker

PoS(LATTICE2021)504

1. Introduction

In the standard model of modern particle physics, the nucleon is known to be a composite particle made of quarks and gluons, and their interactions are described by QCD. Due to the non-perturbative nature of QCD at low energy scales, the nucleon structure that is governed by strong many body problem of the elementary constituents is one of the great challenges of lattice QCD. An appropriate theoretical framework to investigate the nucleon structure is established through the transverse-momentum-dependent parton distributions and the generalized parton distributions, which unify the concepts of parton distributions obtained from the deep inelastic scattering experiments and nucleon elastic form factors. The parton distributions are not only used as inputs for simulations of high energy scattering processes in high energy physics [1], but also play important roles to describe various properties of the nucleon such as proton's single spin asymmetry, hadron tomography, gluons saturation and so on [2, 3].

Apart from the direct calculation of the parton distributions from lattice QCD [4, 5], it is still important to determine the lower moments of the parton distributions associated with twist-2 operators. Since the isovector momentum fraction ($\langle x \rangle_{u-d}$) and the isovector helicity fraction ($\langle x \rangle_{\Delta u - \Delta d}$) are well evaluated from the experimental data, the calculation of these quantities is a benchmark to explore the nucleon structure from lattice QCD. In addition, the precision on the isovector axial-vector coupling (g_A) is greatly improved by the current β-decay measurements with cold and ultracold neutrons [6]. Therefore, it offers an opportunity to pursue the high-precision calculation of g_A in lattice QCD in the context of a benchmark study.

2. Method

Both the lower moments of parton distributions (Twist-2) and the axial-vector (vector) coupling (Local) can be evaluated from the nucleon matrix element of a given bilinear operator, $O_\Gamma = \bar{\psi}\Gamma\psi$ as defined in Table 1.

Table 1: The correspondence of the quantities and operators in the matrix elements[7].

Type of operator	Local		Twist-2	
Observable	g_V (vector)	g_A (axial-vector)	$\langle x \rangle_{u-d}$ (unpolarized)	$\langle x \rangle_{\Delta u - \Delta d}$ (polarized)
Γ	γ_4	$\gamma_i\gamma_5$	$\gamma_4 \overleftrightarrow{D}_4 - \frac{1}{3}\sum_k \gamma_k \overleftrightarrow{D}_k$	$\gamma_3 \overleftrightarrow{D}_4 + \gamma_4 \overleftrightarrow{D}_3$

In general, the nucleon matrix elements are evaluated from a ratio of the nucleon three-point function with a given operator O_Γ inserted at $t = t_{\rm op}$ being subject to a range of $t_{\rm snk} > t > t_{\rm src}$, to the nucleon two-point function with a source-sink separation ($t_{\rm sep} = t_{\rm snk} - t_{\rm src}$) as

$$R(t_{\rm sep}, t_{\rm op}) \equiv \frac{C^{\rm 3pt}(t_{\rm op}, t_{\rm sep})}{C^{\rm 2pt}(t_{\rm sep})} \underset{t_{\rm sep} \gg t_{\rm op} \gg 0}{\longrightarrow} \langle 1|O_\Gamma|1\rangle + \mathcal{O}(e^{-t_{\rm sep}\Delta}) + \mathcal{O}(e^{-(t_{\rm sep}-t_{\rm op})\Delta}), \tag{1}$$

where $|i\rangle$ represents the i-th energy eigenstate and $i = 1$ stands for the ground state of the nucleon. If the condition $t_{\rm sep} \gg t_{\rm op} \gg 0$ is satisfied, the desired matrix element $\langle 1|O_\Gamma|1\rangle$ can be read off from an asymptotic plateau, which is independent of a choice of $t_{\rm op}$. Narrower source-sink separation causes systematic uncertainties stemming from the excited states contamination represented by two

terms of $\mathcal{O}(\mathrm{e}^{-t_{\rm sep}\Delta})$ and $\mathcal{O}(\mathrm{e}^{-(t_{\rm sep}-t_{\rm op})\Delta})$, where $\Delta \equiv E_2 - E_1$ denotes a difference between the two energies of the ground state (E_1) and the lowest excited state (E_2).

In this study, the nucleon interpolating operator is constructed by the exponentially smeared quark operators, so as to maximize an overlap with the nucleon ground state as

$$N(t,\vec{p}) = \sum_{\vec{x}\vec{x}_1\vec{x}_2\vec{x}_3} \mathrm{e}^{-i\vec{p}\cdot\vec{x}} \varepsilon_{abc} \left[u_a^T(t,\vec{x}_1) C\gamma_5 d_b(t,\vec{x}_2)\right] u_c(t,\vec{x}_3) \times \Pi_{i=1}^3 \phi(\vec{x}_i - \vec{x})$$
$$\text{with} \quad \phi(\vec{x}_i - \vec{x}) = A\exp(-B|\vec{x}_i - \vec{x}|) \tag{2}$$

where there are two smearing parameters (A, B). Since the condition, $t_{\rm sep} \gg t_{\rm op} \gg 0$ appearing in Eq. (1) is usually not satisfied in practice, the excited states contaminations could not be fully eliminated by tuning smearing parameters.

In order to eliminate the systematic uncertainties, one should calculate the ratio (1) with several choices of $t_{\rm sep}$, and then makes sure whether the evaluated value of the nucleon matrix element does not change with a variation of $t_{\rm sep}$ within a certain precision. This is called the ratio method that is mainly used in this study. Alternatively, there is another method called the summation method [8]. The summation method use a sum of the ratio $R(t_{\rm op}, t_{\rm sep})$ with respect to $t_{\rm op}$ as

$$S(t_{\rm sep}) \equiv \sum_{t_{\rm op}=0}^{t_{\rm sep}} R(t_{\rm op}, t_{\rm sep}) \underset{t_{\rm sep}\gg 0}{\to} \text{const.} + t_{\rm sep}\langle 1|O_\Gamma|1\rangle + \mathcal{O}(\mathrm{e}^{-\Delta t_{\rm sep}}) \tag{3}$$

When more than 3 sets of $t_{\rm sep}$ are carried out in the ratio method, one can also perform the summation method [8], where the matrix element $\langle 1|O_\Gamma|1\rangle$ can be read off from a slope of the linear dependence of $t_{\rm sep}$ as described in Eq. (3). A difference of the central values obtained from the two methods is quoted as a systematic error on the matrix element evaluated from the ratio method in this study.

In order to compare with the experimental values or other lattice results, the *bare matrix element* obtained from the above mentioned methods should be renormalized with the renormalization constants Z_{O_Γ} for each Γ operator in a certain scheme. In this study, for the twist-2 operators, the Regularization Independent MOMentum subtraction (RI/MOM) scheme [9] is used as the intermediate scheme in order to evaluate the renormalization constants Z_{O_Γ} in fully nonperturbative manner. The renormalization constants determined in the RI/MOM scheme are then converted to the $\overline{\rm MS}$ scheme at certain scale μ_0 and evolved to the scale of 2 GeV using the perturbation theory.

In general, the final result of $Z_{O_\Gamma}^{\overline{\rm MS}}(2\text{GeV})$ receives the residual dependence of the choice of the matching scale μ_0. It is true that the perturbative conversion from the RI/MOM scheme to the $\overline{\rm MS}$ scheme produces the residual μ_0 dependence, but the perturbative uncertainty is not a major concern here. There are the other two sources as follows. One stems from lattice discretization errors at higher μ_0, while another is originated from the nonperturbative effect that becomes relevant at lower μ_0 [10–12]. The latter is not so serious if the spatial volume is not so large, because the lower momentums are not accessible in the smaller volume. However, in this study, we use 64^4 lattice, corresponding to a linear spatial extent of 5.5 fm, that is rather large spatial size.

In order to minimize the systematic uncertainties associated with the residual μ_0-dependence,

we used following two types of fitting functional forms as functions of the matching scale μ_0:

$$f_{O_\Gamma}^{\text{Global}}(\mu_0) = \frac{c_{-1}}{(\Lambda^{-1}\mu_0)^2} + c_0 + \sum_{k>0}^{k_{\max}} c_k (a\mu_0)^{2k} \quad \text{and} \quad f_{O_\Gamma}^{\text{IR-trunc.}}(\mu_0) = c_0 + \sum_{k>0}^{k_{\max}} c_k (a\mu_0)^{2k} \tag{4}$$

with c_0 being the μ_0-independent value of $Z_{O_\Gamma}^{\overline{\text{MS}}}(\mu)$ at the renormalization scale $\mu = 2$ GeV. The value of $k_{\max}$ is determined by a χ^2 test for goodness fit, so that $k_{\max} = 3$ is chosen for the former, while $k_{\max} = 1$ is chosen for the later. In the former form, Λ is responsible for a scale associated with the nonperturbative effect. The former is applied for fitting all data, while the latter is used for fitting the data in a restricted range of $\mu_0 \geq \mu$. The discrepancy between the values of c_0 extracted from these fittings is quoted as a systematic error on the renormalization constant $Z_{O_\Gamma}^{\overline{\text{MS}}}(2\text{ GeV})$.

3. Simulation details

We mainly use the PACS10 configurations generated by the PACS Collaboration with the six stout-smeared $\mathcal{O}(a)$ improved Wilson-clover quark action and Iwasaki gauge action at $\beta = 1.82$ and 2.00 corresponding to the lattice spacings of 0.085 fm (coarser) and 0.064 fm (finer) respectively [13–17]. When we compute nucleon two-point and three-point functions, the all-mode-averaging (AMA) technique[18] is employed in order to reduce the statistical errors significantly without increasing computational costs. Two of three lattice ensembles are created with same lattice cutoff, but on different lattice sizes. The smaller volume ensembles are used for the finite volume study on the axial-vector coupling g_A and nucleon elastic form factors, and also used for computing the renormalization constants which are known to be less sensitive to the finite volume effect.

Table 2: Summary of simulation parameters used in this study.

	β	$L^3 \times T$	a^{-1} [GeV]	La [fm]	κ_{ud}	κ_s	M_π [GeV]
128^4 lattice	1.82	$128^3 \times 128$	2.3162(44)	10.9	0.126117	0.124902	0.135
64^4 lattice	1.82	$64^3 \times 64$	2.3162(44)	5.5	0.126117	0.124902	0.138
160^4 lattice	2.00	$160^3 \times 160$	3.0892(25)	10.3	0.12584	0.124925	0.135

4. Numerical results

In this study, we first present the preliminary results for the renormalized values of the isovector momentum fraction ($\langle x \rangle_{u-d}$) and the isovector helicity fraction ($\langle x \rangle_{\Delta u - \Delta d}$), which are calculated only at a single lattice spacing with the 128^4 lattice ensemble. We will later discuss the discretization uncertainties on two specific ratios of g_A/g_V and $\langle x \rangle_{u-d}/\langle x \rangle_{\Delta u - \Delta d}$, which are not renormalized in the continuum limit. These quantities, which are evaluated with both 128^4 and 160^4 lattice ensembles, can be directory compared with the experimental data without renormalization.

4.1 Renormalized values of momentum and helicity fractions from 128^4 lattice ensemble

In order to evaluate $\langle x \rangle_{u-d}$ and $\langle x \rangle_{\Delta u - \Delta d}$, we calculate both the bare nucleon matrix elements of the relevant twist-2 operators and their renormalization constants at lattice spacing of $a = 0.085$ fm.

Table 3: Details of the measurements: time separation ($t_{\rm sep}$), the smearing parameters (A, B), the number of high-precision calculation ($N_{\rm org}$), the number of configuration ($N_{\rm conf}$), the measurements per configuration (N_G) and the total number of the measurement ($N_{\rm meas} = N_{\rm conf} \times N_G$), respectively.

	$t_{\rm sep}/a$	Smearing parameters	$N_{\rm org}$	N_G	$N_{\rm conf}$	$N_{\rm meas}$
128^4 lattice	10	$(A, B) = (1.2, 0.16)$	1	128	20	2,560
	12		1	256	20	5,120
	14		2	320	20	6,400
	16		4	512	20	10,240
64^4 lattice	12	$(A, B) = (1.2, 0.14)$	4	256	100	25,600
	14		4	1,024	100	102,400
	16		4	2,048	100	204,800
160^4 lattice	16	$(A, B) = (1.2, 0.11)$	4	64	15	9,210
	19		2	64	15	15,360

As for the calculations of the bare matrix elements, four data sets using $t_{\rm sep}/a = \{10, 12, 14, 16\}$ are calculated and two methods are employed in the extraction of the bare matrix elements. According to the analysis based on the ratio method, we first observed that $t_{\rm sep}/a = \{14, 16\}$ for the unpolarized case and $t_{\rm sep}/a = \{12, 14, 16\}$ for the polarized case are large enough for reducing the excited states contamination in three-point functions with the twist-2 operators respectively. Next, all data sets with four values of $t_{\rm sep}/a$ are used in the summation method in order to estimate the systematic error associated with the excited states contamination in each channel.

The renormalization constants of the local vector and axial-vector currents are obtained with the Schrödinger functional scheme at vanishing quark masses as $Z_V = 0.95153(76)(1487)$ and $Z_A = 0.9650(68)(95)$ [19], while the renormalization constants of the twist-2 operators are evaluated in the RI/MOM scheme as described in Sec. 2.

Table 4: List of error sources in the renormalized nucleon matrix elements with the twist-2 operators.

	List of errors (%)					
	Momentum fraction $\langle x \rangle_{u-d}$			Helicity fraction $\langle x \rangle_{\Delta u - \Delta d}$		
Error source	Total	Bare value	Z-factor	Total	Bare value	Z-factor
Statistical	5.30	4.60	2.52	4.39	3.49	2.91
Systematic	31.1	19.5	24.5	24.0	3.49	22.5

As shown in Fig 1, we compare our preliminary results of the renormalized values of $\langle x \rangle_{u-d}$ (left panels) and $\langle x \rangle_{\Delta u - \Delta d}$ (right panels) with the values obtained from recent lattice QCD calculations (upper panels) and global QCD analyses of experimental data (lower panels). The central values of our results are well within gray bands corresponding to the experimental values given by global fit determinations [4, 5]: $\langle x \rangle_{u-d} = 0.155(5)$ and $\langle x \rangle_{\Delta u - \Delta d} = 0.199(16)$. It is worth mentioning that our statistical precisions are also comparable to the global QCD analyses. This indicates that lattice QCD is partially qualified to directly investigate the parton distributions as an alternative to actual experiments. However, it should be kept in mind that our preliminary results of $\langle x \rangle_{u-d}$ and $\langle x \rangle_{\Delta u - \Delta d}$ still have large systematic errors as shown in Tab. 4. As for the bare matrix elements,

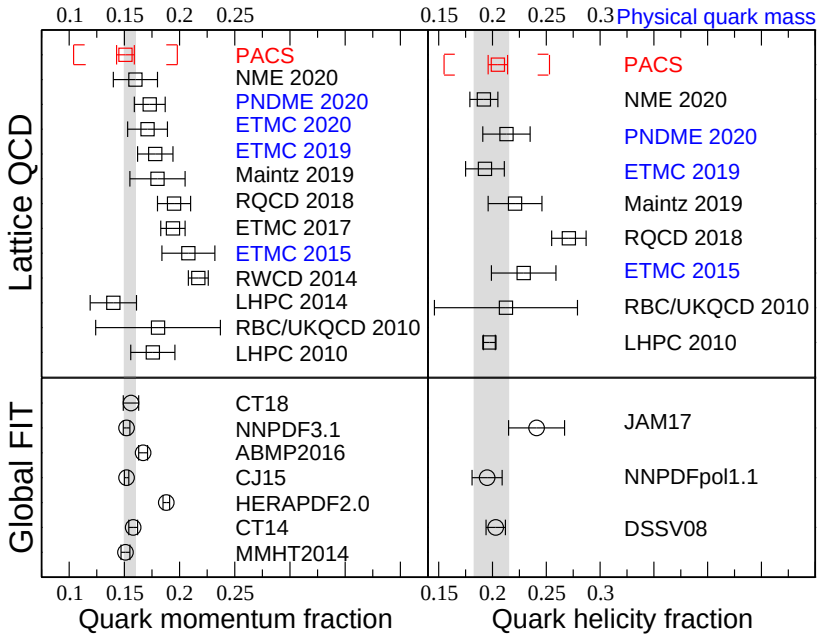

Figure 1: Comparison of recent lattice QCD calculations (upper panels) and global QCD analyses of experimental data (lower panels). The red symbols represent our preliminary results. The error bars denote their statistical errors only, while the outer brackets with our results represent the total errors including the systematic one. The gray bands correspond to the values of an average given by global fit determinations [4, 5].

discrepancies between the results obtained from the two methods are quoted as a systematic error stemming from the excited states contaminations. It is found that for the unpolarized case the evaluated systematic error with the present sets of $t_{\rm sep}/a = \{10, 12, 14, 16\}$ is larger than the statistical one, while the statistical and systematic uncertainties are also comparable in the polarized case. A further calculation with the larger choice of $t_{\rm sep}/a(> 16)$ is required to reduce this particular uncertainty. The largest error on $\langle x\rangle_{u-d}$ ($\langle x\rangle_{\Delta u-\Delta d}$) is the systematic uncertainty in determination of the renormalization constants. This systematic error was evaluated by a difference between the results obtained by two fitting procedures with Eqs. (4) which have different ways to treat the residual μ_0-dependence in smaller μ_0 region. As shown in Tab. 4, the total systematic errors, which are about 6 times larger than the total statistical errors, are dominated by the systematic errors on the renormalization constants. To reduce the total systematic error, the RI/SMOM scheme that was used for determination of the renormalization constant for the local operators [20], could be useful even for the twist-2 operators.

4.2 Ratios of g_A/g_V and $\langle x\rangle_{u-d}/\langle x\rangle_{\Delta u-\Delta d}$ from 128^4 and 160^4 lattice ensembles

We next present our preliminary results of g_A/g_V and $\langle x\rangle_{u-d}/\langle x\rangle_{\Delta u-\Delta d}$ obtained from both 128^4 and 160^4 lattice ensembles, since the renormalization constants are not yet evaluated at finer lattice spacing. In Fig 2, we first shows the $t_{\rm sep}$ dependence of the ratios of g_A/g_V (left panel) and $\langle x\rangle_{u-d}/\langle x\rangle_{\Delta u-\Delta d}$ (right panel), both of which are evaluated with the ratio method. All three ensembles that include the 64^4 lattice ensemble are used to calculate the values of g_A/g_V, while only the 128^4 and 160^4 lattice ensembles are used to calculate the value of $\langle x\rangle_{u-d}/\langle x\rangle_{\Delta u-\Delta d}$.

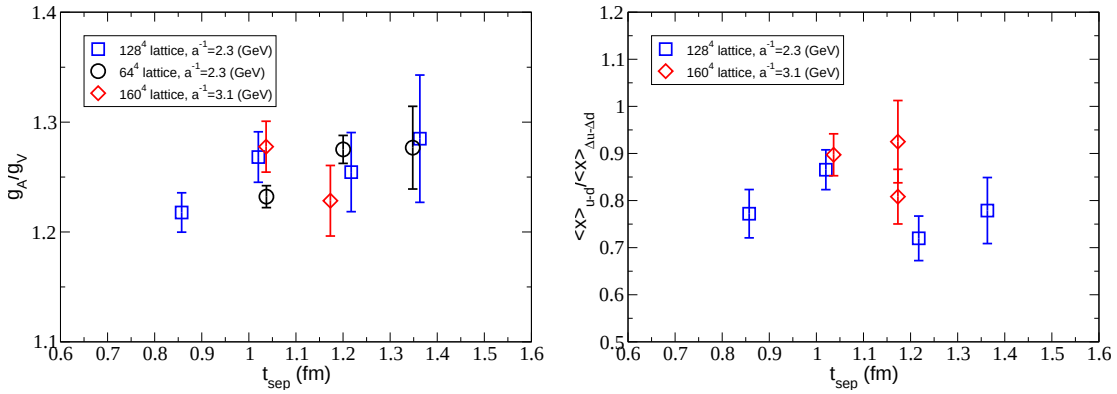

Figure 2: Ratios of bare values of g_A and g_V (left), and $\langle x \rangle_{u-d}$ and $\langle x \rangle_{\Delta u - \Delta d}$ (right) as a function of $t_{\rm sep}$.

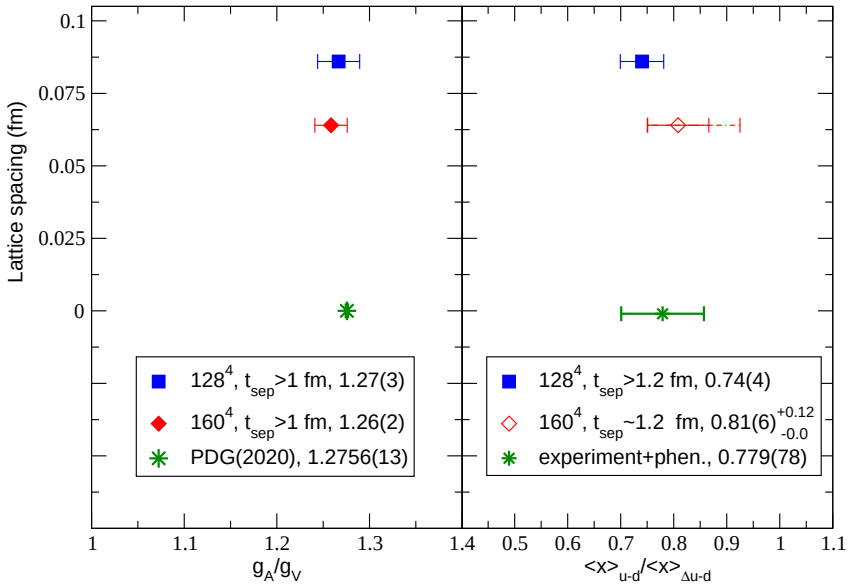

Figure 3: Preliminary results of g_A/g_V and $\langle x \rangle_{u-d}/\langle x \rangle_{\Delta u - \Delta d}$ obtained from 128^4 and 160^4 lattice ensembles. The value of $\langle x \rangle_{u-d}/\langle x \rangle_{\Delta u - \Delta d}$ obtained from the 160^4 lattice ensemble (open diamond symbol) receives a large uncertainty regarding the fit range dependence that is represented by dashed error bar.

At first glance, the conditions of $t_{\rm sep} \geq 1$ fm for the case of g_A/g_V and $t_{\rm sep} \geq 1.2$ fm for the case of $\langle x \rangle_{u-d}/\langle x \rangle_{\Delta u - \Delta d}$ can be read off from the 128^4 lattice results, in order to keep the systematic uncertainties stemming from the excited states contamination smaller than the statistical ones. As for the results of g_A/g_V, the preliminary results from the 160^4 lattice ensemble show a consistent observation, though the higher accuracy results from the 64^4 lattice ensemble reveal that the data of $t_{\rm sep} \approx 1$ fm is slightly deviated from the results for $t_{\rm sep} \geq 1.2$ fm.

On the other hand, the preliminary results of $\langle x \rangle_{u-d}/\langle x \rangle_{\Delta u - \Delta d}$ from the 160^4 lattice ensemble have not shown any obvious trend of $t_{\rm sep}$ dependence, since a large uncertainty still remains for the data given with $t_{\rm sep} \approx 1.2$ fm. As shown in the right panel of Fig 2, two data points, which are obtained from two fitting ranges used in the ratio method, are plotted at $t_{\rm sep} \approx 1.2$ fm. The upper data point agrees the data obtained with $t_{\rm sep} \approx 1.0$ fm, while the lower data point follows the trend

observed in the 128^4 lattice results. It is difficult to draw any firm conclusion whether the systematic uncertainties stemming from the excited states contamination are under control for the 160^4 lattice results of $\langle x \rangle_{u-d}/\langle x \rangle_{\Delta u-\Delta d}$ within the current statistics. Therefore, in the later discussion, we use the lower data point of $t_{\rm sep} \approx 1.2$ fm for the 160^4 lattice result, while a systematic error estimated by a difference between two data points is also quoted.

We next examine the lattice discretization uncertainties on g_A/g_V and $\langle x \rangle_{u-d}/\langle x \rangle_{\Delta u-\Delta d}$ using the results obtained at two lattice spacings as shown in Fig 3. According to what we discussed using Fig 2, in the case of g_A/g_V there is no appreciable $t_{\rm sep}$ dependence in the large volume results obtained from both lattice ensembles if $t_{\rm sep} \approx 1.0$ fm is satisfied. Therefore, we simply use the combined results with $t_{\rm sep}/a = \{12, 14, 16\}$ for the 128^4 lattice and $t_{\rm sep}/a = \{16, 19\}$ for the 160^4 lattice in the left panel of Fig 2. Both results at two lattice spacings reproduce the experimental value [6] within their statistical errors. This indicates that the lattice discretization uncertainties on the renormalized value of g_A are smaller than their statistical uncertainty of less than 2%.

As for the quantity of $\langle x \rangle_{u-d}/\langle x \rangle_{\Delta u-\Delta d}$, although the 128^4 lattice result obtained at the coarser lattice spacing shows better agreement with the experimental values [4, 5], the large systematic error remains for the preliminary result obtained from the 160^4 lattice ensemble. Needless to say, further reduction of both statistical and systematic errors is needed for the 160^4 lattice results.

5. Summary

We have calculated the renormalized values of $\langle x \rangle_{u-d}$ and $\langle x \rangle_{\Delta u-\Delta d}$ at a single lattice spacing of 0.085 fm, and also the two specific ratios of g_A/g_V and $\langle x \rangle_{u-d}/\langle x \rangle_{\Delta u-\Delta d}$ at two lattice spacings of 0.085 fm and 0.064 fm , using the PACS10 gauge configurations. This work is a benchmark to explore the nucleon structure from lattice QCD calculations. First, we have succeeded in reproducing global QCD analyses of experimental data for both quantities of $\langle x \rangle_{u-d}$ and $\langle x \rangle_{\Delta u-\Delta d}$ with high statistical precision using the 128^4 lattice ensemble. However, it is worth remarking that the large systematic uncertainties remain in determination of the renormalization constants. In future project, instead of the RI/MOM scheme, the RI/SMOM scheme will be able to be used even for the twist-2 operators. Since the renormalization constants are not yet evaluated at the finer lattice spacing, we simply evaluate two ratios of g_A/g_V and $\langle x \rangle_{u-d}/\langle x \rangle_{\Delta u-\Delta d}$, which are not renormalized in the continuum limit. Therefore, we can compare our results of the ratios with the experimental results without the renormalization constants. As for the case of g_A/g_V, both results at two lattice spacings well reproduce the experimental value within their statistical errors. This indicates that the lattice discretization uncertainties on the renormalized value of g_A are smaller than their statistical uncertainty of less than 2%. As in the case of g_A/g_V, the results of $\langle x \rangle_{u-d}/\langle x \rangle_{\Delta u-\Delta d}$ obtained from the 128^4 and 160^4 lattice ensembles reproduce the experimental data, though the large systematic error remains for the preliminary result of obtained from the 160^4 lattice ensemble.

Acknowledgement

Numerical calculations in this work were performed on Oakforest-PACS in Joint Center for Advanced High Performance Computing (JCAHPC) and Cygnus in Center for Computational Sciences at University of Tsukuba under Multidiscilinary Cooperative Research Program of Center for

Computational Sciences, University of Tsukuba, and Wisteria/BDEC-01 in the Information Technology Center, The University of Tokyo. This research also used computational resources through the HPCI System Research Projects (Project ID: hp170022, hp180051, hp180072, hp180126, hp190025, hp190081, hp200062, hp200188, hp210088) provided by Information Technology Center of the University of Tokyo and RIKEN Center for Computational Science (R-CCS). The calculation employed OpenQCD system[1]. This work was supported in part by Grants-in-Aid for Scientific Research from the Ministry of Education, Culture, Sports, Science and Technology(Nos. 18K03605, 19H01892).

References

[1] O. Turkot [H1 and ZEUS], PoS **LeptonPhoton2019** (2019), 077.

[2] H. -W. Lin *et a.*, Phys. Rev. Lett. **120** (2018) 12502.

[3] R. Abdul Khalek *et al.*, arXiv:2103.05419v2(2021).

[4] M. Constantinou *et al.*, arXiv:2006.08636v2(2020).

[5] H.-W. Lin *et al.*, Prog. Part. Nucl. Phys. **100** (2018), 107-160

[6] B. Märkisch *et al.*, Phys. Rev. Lett. **122** (2019) 242501, 1812.04666.

[7] Y. Aoki *et al.*, Phys. Rev. D **82** (2010) 014501.

[8] A. Adbel-Rehim *et al.*, Phys. Rev. D **92** (2015) 114513.

[9] G. Martinelli *et al.*, Nucl. Phys. B **445** (1995) 81.

[10] Y. Aoki, PoS LATTICE 2009, 012(2010).

[11] Y. Aoki, P. A. Boyle, N. H. Christ *et al.*, Phys. Rev. D **78** (2008) 054510.

[12] P. Boucaud *et al.*, Phys. Rev. D **74** (2006) 034505.

[13] Y. Iwasaki, (2011), UTHEP-118, arXiv:1111.7054 [hep-lat].

[14] K. I. Ishikawa *et al.*, Phys. Rev. D **99** (2019) 014504.

[15] K. I. Ishikawa *et al.*, Phys. Rev. D **100** (2019) 094502.

[16] E. Shintani *et al.*, Phys. Rev. D **94** (2019) 014510. (Erratum; Phys. Rev. D **102** (2020) 019902.)

[17] E. Shintani and Y. Kuramashi, Phys. Rev. D **100** (2019) 034517.

[18] G. von Hippel, T. D. Rae, E. Shintani, and H. Wittig, Nucl. Phys. B **914** (2017) 138.

[19] K. I. Ishikawa *et al.* [PACS], PoS **LATTICE2015** (2016) 271.

[20] N. Tsukamoto *et al.*, PoS **LATTICE2019** (2020), 132.

[1] http://luscher.web.cern.ch/luscher/openQCD/